PNAS RESEARCH ARTICLE | CHEMISTRY

Abiotic origin of the citric acid cycle intermediates

Mason McAnally[a,b], Jana Bocková[c], Andrew M. Turner[a,b], Nana Hara[a,b], Daria Mikhnova[a,b], Cornelia Meinert[c,1], and Ralf I. Kaiser[a,b,1]

Edited by Nigel J. Mason, University of Kent, Canterbury, United Kingdom; received January 24, 2025; accepted March 22, 2025 by Editorial Board Member Stephen J. Benkovic

The molecular framework for protometabolism—chemical reactions in a prebiotic environment preceding modern metabolism—has remained unknown in evolutionary biology. Mono-, di-, and tricarboxylic acids that comprise contemporary metabolism, such as the Krebs cycle, are of particular prebiotic relevance and are theorized to predate life on Earth. Researchers have struggled to unravel the molecular origins of respiration, with theories pointing toward abiotic origins later co-opted by the earliest living organisms; however, the molecular network of these molecules has remained elusive. Recent detections of carboxylic acids linked to the Krebs cycle on the Ryugu asteroid and Murchison meteorite rekindled interest in their extraterrestrial origins. Replicating conditions analogous to the environment of dense molecular clouds in laboratory simulation experiments, our work provides compelling evidence on the abiotic synthesis of the complete suite of biorelevant molecules central to the Krebs cycle. The opportunity for these biomolecules forming in deep space could provide molecular origins of protometabolism on early Earth and also provide the molecular feedstock to worlds beyond our own.

citric acid cycle | prebiotic chemistry | astrochemistry | interstellar ice

Significance

The chemistry of cold molecular clouds is remarkably rich in complex organic molecules. By replicating the conditions of ice-coated nanoparticles in these cold regions of space, laboratory simulation experiments provide compelling evidence on the synthesis of the complete set of organics of the citric acid cycle in interstellar analog ices exposed to ionizing radiation. These findings illustrate a plausible starting point for developing molecular precursors to life in deep space in conjunction with the incorporation of these building blocks into solar systems, as evidenced by Ryugu and Murchison, potentially laying the groundwork for metabolic evolution and the *Origins of Life*.

The Krebs cycle—also called citric acid cycle (Fig. 1)—is fundamental to all respiring organisms and provides a metabolic pathway synthesizing precursors to amino acids and supporting cellular bioenergetics (1). The reliance of all contemporary lifeforms on the Krebs cycle points to its adoption by the earliest living organisms on Earth. Prevailing theories on the origins of protometabolic processes inferred that through terrestrial (geo) chemical alteration, the molecular components of the Krebs cycle were accessible to the earliest lifeforms on Earth (2, 3). If these molecules are required to form the earliest metabolic systems, an abiotic synthesis of these molecules would be the key to setting the stage for the advent of biochemical evolution. Although terrestrial alterations of precursors to the molecular material of the Krebs cycle have been a focus of attention for the last decades (3–8), the proposed pathways are plagued with exceptionally specific reaction conditions such as elevated temperatures (323 to 343 K) (3, 4, 8) or require strong oxidizing agents (peroxydisulfate, $S_2O_8{}^{2-}$) (3). Krebs cycle intermediates were detected in the Murchison meteorite (9) and in returned samples from the Ryugu carbonaceous asteroid collected by the Hayabusa2 mission (10). The identification of biomolecules such as citric acid **2** and pyruvic acid **1** that are connected to the Krebs cycle in extraterrestrial matter illustrates a plausible starting point for the development of molecular precursors to life in deep space in conjunction with a delivery of these building blocks to early Earth as a likely source of chemical feedstocks for the *Origins of Life* (9). However, the fundamental processes producing the full suite of biochemicals connected to the Krebs cycle in deep space have remained elusive.

Since the biorelevant organic compounds in carbonaceous chondrites such as Murchison are partly sourced from interstellar grains (11, 12)—galactic cosmic ray-processed ice-coated nanoparticles in molecular clouds—the synthesis of biomolecules on these nanoparticles within dense molecular clouds could account for the comprehensive range of molecular material required for the Krebs cycle. Interstellar grains in dense molecular clouds accumulate an icy mantle through gas accretion providing a medium for condensed-phase chemical reactions. However, temperatures prevailing in molecular clouds (10 K) limit thermochemistry to tunneling (13); alternatively, nonequilibrium chemical reactions can be initiated by ionizing irradiation such as GCRs and vacuum ultraviolet (VUV) light (14). Biomolecules such as sugars and amino acids have been reported previously in space simulation experiments exploring the abiotic generation of key compounds on interstellar grains at temperatures and doses characteristic of cold molecular clouds (15–18). However, a detailed investigation into the formation of the complete suite of complex organic molecules of the Krebs cycle under interstellar conditions on ice-coated nanoparticles has not been accomplished. However, this endeavor

Author affiliations: [a]Department of Chemistry, University of Hawaii at Mānoa, Honolulu, HI 96822; [b]W. M. Keck Laboratory in Astrochemistry, University of Hawaii at Mānoa, Honolulu, HI 96822; and [c]UMR 7272 CNRS, Institut de Chimie de Nice, Université Côte d'Azur, Nice 06108, France

Author contributions: C.M. and R.I.K. designed research; M.M., J.B., A.M.T., and N.H. performed research; M.M., J.B., and D.M. analyzed data; and M.M. wrote the paper.

The authors declare no competing interest.

This article is a PNAS Direct Submission. N.J.M. is a guest editor invited by the Editorial Board.

[1] To whom correspondence may be addressed. Email: Cornelia.MEINERT@univ-cotedazur.fr or ralfk@hawaii.edu.

This article contains supporting information online at https://www.pnas.org/lookup/suppl/doi:10.1073/pnas.2501839122/-/DCSupplemental.

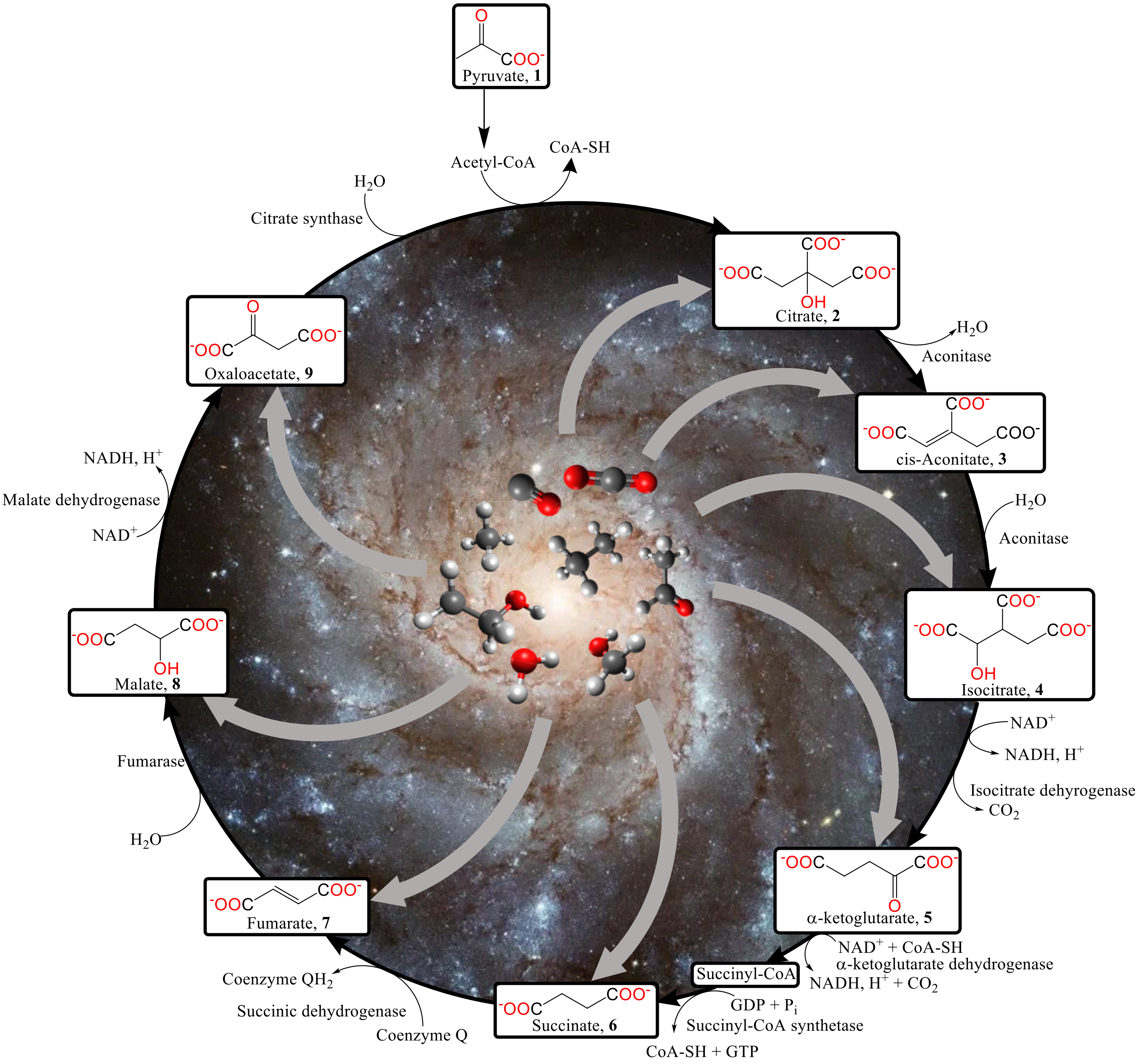

Fig. 1. Overview of the Krebs cycle in contemporary biochemistry and reactant molecules (CH_4, CO_2, CO, H_2O, CH_3OH, C_2H_6, CH_3CH_2OH, CH_3CHO) utilized in the interstellar ices to synthesize key molecular components of the cycle in our experiments. Carbon (gray), hydrogen (white), and oxygen (red) are critical elements in biology and interstellar ices. These known interstellar molecules are subjected to the harsh conditions of dense molecular clouds such as galactic cosmic rays (GCRs) and can produce the full suite of complex organic molecules of the Krebs cycle.

is essential not only to understand the origins of biomolecules found in Murchison and Ryugu but also to establish whether such vital materials for the Krebs cycle and for life itself are produced extensively throughout the interstellar medium (ISM). The James Webb Space Telescope (JWST) has provided exciting data that allow cataloging of simple molecules observed in interstellar ices including methane (CH_4), carbon dioxide (CO_2), water (H_2O), carbon monoxide (CO), methanol (CH_3OH) (19). The processing of these species in interstellar icy mantles by GCRs could produce the organics found in the Krebs cycle. Once these molecules have formed, they can remain (partly) on the grains during the collapse of the molecular cloud toward hot molecular cores as temperatures increase up to 300 K as protostars and protoplanetary disks accrete from the ice and dust that comprised the molecular cloud (20, 21). During this collapse stage, material can become integrated into small celestial bodies and, upon delivery to early Earth, could provide a molecular framework for the first metabolic pathways.

Here, we present the unambiguous detection of the full suite of biorelevant molecules central to the Krebs cycle synthesized in low-temperature interstellar analog ices at 10 K under conditions mimicking typical ages of molecular clouds of up to 10^7 y. The key organics of the Krebs cycle—pyruvic acid ($CH_3COCOOH$ **1**), citric acid ($HOC(CH_2COOH)_2COOH$ **2**), *cis*-aconitic acid ($HOC(O)CH_2C(COOH){=}CHCOOH$ **3**), isocitric acid ($HOC(O)CH\ (CH_2COOH)C(OH)COOH$ **4**), *α*-ketoglutaric acid ($HOC(O)C(O)CH_2CH_2COOH$ **5**), succinic acid ($HOC(O)CH_2CH_2COOH$ **6**), fumaric acid ($HOC(O)CH{=}CHCOOH$ **7**), malic acid ($HOC(O)\ CH_2CH(OH)COOH$ **8**), and oxaloacetic acid ($HOC(O)C(O)CH_2COOH$ **9**) (Fig. 1)—were synthesized by exposing discrete interstellar model ices carrying astronomically known reactants (CH_4, CO, CO_2, CH_3OH, H_2O) (19) and their first-generation radiolysis products [ethanol, CH_3CH_2OH (22); ethane, C_2H_6 (23); and acetaldehyde, CH_3CHO (24)] to proxies of GCRs (*Materials and Methods*). These acids represent the respective anions found in the Krebs cycle at physiological pH. Fourier transform infrared (FTIR) spectroscopy was utilized to trace the chemical changes and the emergence of critical functional groups connected to the complex organics during the irradiation, whereas the temperature-programmed desorption (TPD) simulates the temperature increase during molecular cloud collapse toward protostar formation with temperatures of up to 300 K (21). The resultant residues were extracted and derivatized for analysis of individual molecules via two-dimensional gas chromatography in conjunction with a time-of-flight mass spectrometer (GC×GC–TOF-MS) (*Materials and Methods*). The synthesis and detection of these complex organics not only reveal fundamental synthetic routes in the Murchison meteorite and the Ryugu asteroid but also uncover a cosmic connection between astrophysical processes, nonequilibrium chemical reactions, and the molecular underpinnings of life itself—providing compelling evidence that the molecular precursors to life and most specifically to the Krebs cycle may have been forged in the icy mantles of interstellar space, poised for delivery to early Earth, where they could spark the birth of metabolic processes.

Results

Fourier Transform Infrared Spectroscopy. Infrared spectroscopy was employed to monitor chemical changes in the ices during irradiation and throughout the TPD phase as the ice was heated to 320 K. Spectra were collected and averaged in 2 min intervals for each ice experiment. A full list of all 12 experiments conducted along with the experimental parameters can be found in Tables S1 and S2, respectively. Each experiment exploited carbon-13 isotopologs to discriminate from potential terrestrial contamination. Here, we present the simplest ice system ($^{13}CH_4$/$^{13}CO_2$, 5,000 nA, 5 h) as a prototype dataset to illustrate the transition from pristine ices to radical formation, the resultant functional groups of the irradiation, and the functional groups that remain at 320 K (Fig. 2). After the deposition of the $^{13}CH_4$/$^{13}CO_2$ ice, FTIR revealed fundamental vibrational modes belonging to $^{13}CH_4$ such as the symmetric stretching mode (ν_1) at 2,905 cm^{-1}, the asymmetric stretching mode (ν_3) at 3,000 cm^{-1}, and the deformation mode (ν_4) at 1,296 cm^{-1} as well as other combination or vibrational overtones (*SI Appendix*, Table S3) (23).

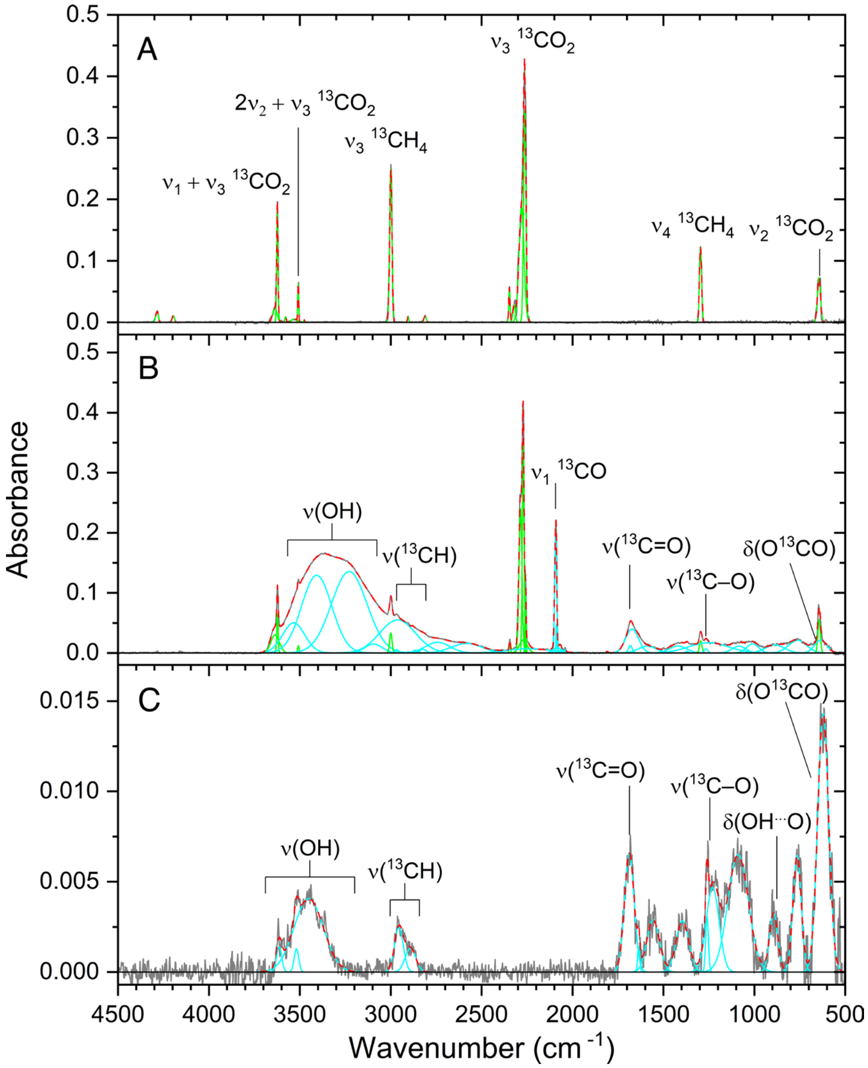

Fig. 2. FTIR spectra of methane (CH_4)/carbon dioxide (CO_2) ices before irradiation (*A*), after irradiation (*B*), and of the residue (*C*) obtained after annealing the exposed ices to 320 K. The spectra are deconvoluted to reveal functional groups related to the reagents (green) and products (cyan).

Carbon dioxide-^{13}C was detected via the asymmetric stretch at 2,270 cm^{-1} (ν_3), the bending mode (ν_2) at 644 cm^{-1}, and two combination bands at 3,630 ($v_1 + v_3$) and 3,509 ($2v_2 + v_3$) (25).

During the irradiation, a critical radical—the HO^{13}CO (hydroxycarbonyl) radical and fundamental molecular building block of all carboxylic acids—was detected by the ^{13}C=O vibrational mode at 1,809 cm^{-1} during the first 10 min of the radiation exposure. This peak remains visible for the full duration of irradiation and contains the connectivity—functional group—and reactivity critical in forming larger carboxylic acids in the network. Following the irradiation, prominent peaks corresponding to carboxylic acid functional groups were observed in the ice, including ^{13}C–O stretching modes or out-of-plane OH bending modes at 1,266 cm^{-1} and 1,252 cm^{-1}, ^{13}C=O stretching at 1,682 to 1,589 cm^{-1}, and new OH stretching modes from 3,534 to 2,962 cm^{-1} (26). Due to the enhanced hydrogen bonding of acid products in the ice matrix, red-shifted O–H stretching modes are detected at 2,582 and 2,242 cm^{-1} (26). Further, the vibrational mode at 887 and 762 cm^{-1} denotes intramolecular hydrogen bonding bending modes of carboxylic acids (26). New ^{13}C–H stretching modes emerge at 2,967, 2,880, 2,864, and 2,824 cm^{-1} coupled with new $^{13}CH_2/^{13}CH_3$ deformations at 1,420 and 1,370 cm^{-1} denoting new alkyl groups in the ice (26). Additionally, a ^{13}C=^{13}C vibrational mode consistent with *cis*-aconitic acid **3** and fumaric acid **7** is found at 1,500 cm^{-1} (26). Finally, small molecules such as ^{13}CO (ν_1, 2,093 cm^{-1}) (25) and H_2O (ν_1/ν_3, 3,534 to 2,962 cm^{-1}; ν_2, 1,673 cm^{-1}) (27) were generated by the radiation exposure.

After the ices were warmed to 320 K, the resulting residue was analyzed spectroscopically to detect any remaining organic material on the substrate (Fig. 2 and *SI Appendix*, Table S5). The resulting spectra revealed peaks corresponding to mono-, di-, and tricarboxylic acids, as well as unsaturated carboxylic acids. A distinct set of O–H stretching modes at 3,614, 3,519, and 3,451 cm^{-1} is observed in the residue along with ^{13}C–H stretching at 2,955 and 2,891 cm^{-1}, ^{13}C=O stretching at 1,688 and 1,636 cm^{-1}, $^{13}CH_3$ deformation at 1,396 cm^{-1}, and ^{13}C–O stretching or the O–H out-of-plane bending at 1,260 and 1,229 cm^{-1} (26). The presence of carboxylic acids is further supported by the presence of an O–^{13}C–O bending vibration at 621 cm^{-1} and the OH···O intramolecular bend at 894 and 765 cm^{-1} (26). The prominent ^{13}C=^{13}C stretching mode at 1,557 cm^{-1} provides the possibility that unsaturated hydrocarbons like fumaric **7** and *cis*-aconitic **3** acid still remain on the substrate at 320 K (26). These functional groups are observed in each irradiated ice experiment (Experiments 2 to 12; *SI Appendix*, Tables S1 and S2) with ^{13}C=O stretching, OH stretching, and ^{13}C–O stretching being the most prominent features in the spectra. By comparison, the residue that remained after the $^{13}CH_4/^{13}CO_2$ ice was irradiated at 5,000 nA for 5 h revealed additional vibrational modes than the same ice mixture irradiated at 2,000 nA for 1 h. Functional groups associated with carboxylic acids are more intense in this high dose experiment compared to the low dose, denoting dose-dependent formation of COMs and additional trapping of carboxylic acids by the residue. Further details on vibrational assignments in additional ice experiments can be found in *SI Appendix*, Figs. S1–S11 and Tables S3.

Although FTIR allows the identification of crucial radicals such as HO^{13}CO and reveals the formation of functional groups, it fails to catalog individual carboxylic acids. Therefore, considering this shortcoming, additional analytical techniques were exploited to unambiguously identify discrete acids belonging to the Krebs cycle.

Two-Dimensional Gas Chromatography Time-of-Flight Mass Spectrometry. The solid residues were analyzed for individual molecules associated with the Krebs cycle. Samples were extracted using high-purity water, dried under a nitrogen stream, and derivatized for two-dimensional gas chromatography time-of-flight mass spectrometry (GC×GC–TOF-MS) analysis (Fig. 3). Each sample was compared against a procedural blank (*SI Appendix*, Figs. S12–S14) to confirm that the products were formed from the radiation exposure thus excluding possible contamination. A sophisticated discrimination of the products from contaminations was also achieved by employing isotopically labeled reagents ($^{13}CH_4$, $^{13}CO_2$, ^{13}CO, $^{13}CH_3OH$, $^{13}C_2H_6$) shifting observed mass-to-charge (*m/z*) ratios by 1 amu per carbon atom. Overall, each sample (excluding the blank) contained the full suite of biological intermediates belonging to the Krebs cycle (1–9). Each molecule was identified by comparing dual retention times ($R_{t1} \times R_{t2}$) as well as the mass spectra of the *t*-butyldimethylsilyl derivative (M^+) main loss channels (CH_3, M–15$^+$; C_4H_9, M–57$^+$). For example, derivatized fumaric acid **7** has a parent mass-to-charge of M^+ = 348 *m/z* and was detected via the methyl loss channel $(M–15)^+$ = 333 *m/z* and the *t*-butyl loss channel *m/z* = 291 (*SI Appendix*, Figs. S12 and S13).

A quantification of the products was achieved through the use of an external calibration curve for each individual carboxylic acid in combination with an internal standard (methyl laurate, $C_{13}H_{26}O_2$) to account for any instrumental bias. This approach revealed that larger acids (C_6; *cis*-aconitic acid **6**, citric acid **2**, and isocitric acid **4**) were up to two orders of magnitude lower in concentration than smaller acids (C_4) such as malic acid **8** (Fig. 4 and Table 1). Relative concentrations of the species reveal two major acids that dominate the ices: malic **8** and oxaloacetic acid **9**. Among the larger acids, citric acid **2** has the highest concentration, indicating preferential production over *cis*-aconitic **3** and isocitric **4** acid. Three peaks were observed for α-ketoglutaric acid **5**, attributed to its degradation during derivatization, a well-documented phenomenon (see *SI Appendix* for more details) (28–30). Finally, each residue also contains fumaric **7**, succinic **6**, and pyruvic acid **1** monomers and dimers, thus completing the full suite of acids in the Krebs cycle (Fig. 1).

When the simplest ice reagents are used ($^{13}CH_4/^{13}CO_2$), a strong dose dependence on the production of the carboxylic acids is observed such that lower doses produced 3.7 ppm of malic acid **8**, whereas higher doses increased the concentrations to 22.6 ppm. Dose dependence occurs for all acids, particularly for larger acids like citric acid **2**. Enhancing the complexity of ice reagents ($^{13}C_2H_6$, $^{13}CH_3{}^{13}CHO$, $^{13}CH_3{}^{13}CH_2OH$) shows no significant increase in the production of acids compared with the simplest ice matrix ($^{13}CH_4/^{13}CO_2$), which could suggest that the concentration of $^{13}CO_2$ is a limiting reagent in the production of acids in ices. Alternatively, the ice containing an aldehyde ($^{13}CH_3{}^{13}CHO$) produced the acids similar to that of the low dose $^{13}CH_4/^{13}CO_2$ experiment. By increasing the $^{13}CO_2$ concentration in the $^{13}CH_3{}^{13}CH_2OH/^{13}CO_2/^{13}CH_4$ system (Experiment 8 to 9) from 44 to 50%, the malic acid **8** detected nearly doubled from 16.1 ppm to 30.5 ppm, illustrating the necessity for carbon dioxide in the synthesis of carboxylic acids. By using the infrared spectra to calculate the total molecules processed and utilizing the blank-corrected concentrations from the chromatograms, the total ice-material converted to acids was extracted (Table 1). In the case of the high-dose $^{13}CH_4/^{13}CO_2$ system, this resulted in 22.6 ppm, 0.6 ppm, and 1.3 ppm of malic **8**, *cis*-aconitic **3**, and citric acid **2**, respectively. Malic acid **8** had the highest production in the $^{13}CH_3{}^{13}CH_2OH/^{13}CO_2$ experiment (Experiment 9) suggesting preferential formation in the ice matrix over all other experiments. Citric acid **2** in extracts from Ryugu contained 145.0 ppb (10), while the low-dose $^{13}CH_4/^{13}CO_2$ experiment (Experiment 2)

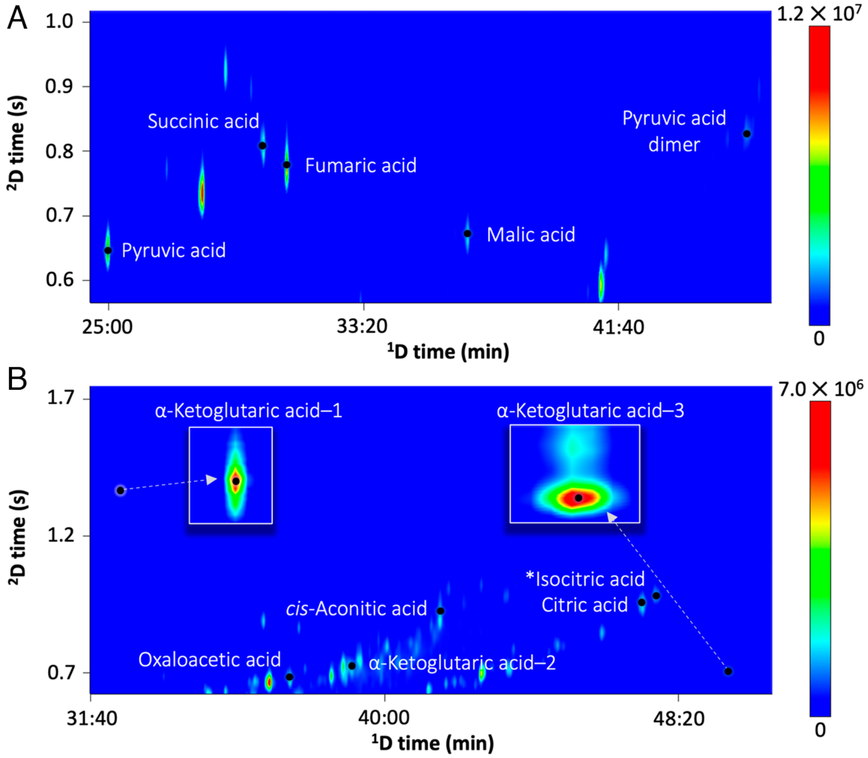

Fig. 3. Pyruvic **1**, succinic **6**, fumaric **7**, malic **8**, oxaloacetic **9**, cis-aconitic **3**, isocitric **4**, citric **2**, α-ketoglutaric **5** acid, and pyruvic acid dimer detected in the residues of exposed interstellar ice analog samples. Multidimensional gas-chromatograms of tBDMS derivatives of (*A*) ^{13}C-labeled pyruvic **1**, succinic **6**, fumaric **7**, malic **8**, and pyruvic acid dimer and (*B*) ^{13}C-labeled α-ketoglutaric **5**, oxaloacetic **9**, cis-aconitic **3**, citric **2**, and isocitric **4** acids extracted from the exposed $^{13}CH_4/^{13}CO_2$ experiment. In (*A*) m/z 262, 291, 293, 423, and 581 are multiplied by a factor of 100. In (*B*) m/z 421, 436 are multiplied by a factor of 10 and m/z 465 is multiplied by a factor of 100. Note that for α-ketoglutaric acid 5, three peaks were identified in the residue marked as 1 to 3 (*SI Appendix*). *No standard for isocitric acid **4** was available.

yielded 100 ppb of citric acid **2** in the ice, suggesting that the lower dose accurately replicates the concentrations observed in Ryugu and may provide a reliable model for the formation scenario of carboxylic acids found on the asteroid.

These data provide compelling evidence that every single molecule (1–9) involved in the Krebs cycle can be produced from a wide range of starting materials known to exist in the ISM. Moreover, the simplest ice experiment—$^{13}CH_4/^{13}CO_2$—indicates that this process is ubiquitous across ice-coated nanoparticles of cold molecular clouds, particularly in regions where interstellar icy mantles are rich in methane and carbon dioxide (31). These findings are integral to understanding recent detections of malic **8**, pyruvic **1**, citric **2**, and succinic **6** acid in Ryugu (10) as part of the Hayabusa2 mission. Further, they explain the prevalence of pyruvic acid **1** along with its dimer and other molecules such as citric **2**, isocitric **4**, and α-ketoglutaric **5** acid found in carbonaceous chondrites such as Murchison (9). This technique enables the unambiguous identification of individual molecules belonging to the Krebs cycle that could persist during the warm-up phase in hot molecular cores before integrating into small celestial bodies. Once these bodies are delivered to Earth such as in the case of Murchison (9), they could provide the essential feedstock for the earliest protometabolic processes (Fig. 4).

Discussion

Since the full suite of intermediates belonging to the Krebs cycle has been detected in the residues, we now present possible formation mechanisms of these organics. The mechanisms are informed in part by the overall structure of the molecules, the reagent used within the ice, functional groups observed spectroscopically, and finally, the identification of radical intermediates during the irradiation. The radicals found here (*SI Appendix*, Fig. S15) illustrate possible starting points for neutral–radical and radical–radical recombination that could yield higher-order carboxylic acids such as those in the Krebs cycle. The identification of the $HO^{13}CO$ radical in particular illustrates the formation of reactive intermediates to carboxylic acids. The path from this point is dependent on the reagents available in the system. First, we present the formation of the smallest carboxylic acid, pyruvic acid **1**, within the ice to highlight a versatile process for the production of acids in interstellar analog ices.

We begin with the breakdown of the reagent components in the $^{13}CH_4/^{13}CO_2$ ice to radicals. For convenience, the energetics are presented as their carbon-12 isotopologs. Two species are found in situ via FTIR: the HOCO radical and carbon monoxide. Ionizing radiation interacting with methane (CH_4) (23) and carbon dioxide (CO_2) (32) induces cleavage of the C–H and C=O bonds in an endoergic reaction, forming the methyl radical (CH_3; $\Delta_RG = +432$ kJ mol^{-1}) (33) and carbon monoxide (CO; $\Delta_RG = +526$ kJ mol^{-1}) (33), respectively (Reaction 1 and 2). Hydrogen atoms released in the decomposition of methane are suprathermal in the ice matrix allowing the atoms to overcome entrance barriers to, e.g., addition to double or triple bonds. Here, neutral–radical addition of the hydrogen atom to an oxygen in carbon dioxide facilitates the production of the hydroxycarbonyl radical in an exoergic ($\Delta_RG = -4$ kJ mol^{-1}) (33) reaction (Reaction 3). Subsequently, hydrogen atoms can react with newly formed carbon monoxide to form the formyl radical (HCO, Reaction 4; $\Delta_RG = -61$ kJ mol^{-1}) (33). Involving barrierless radical–radical recombination, the formyl radical can react with methane to yield acetaldehyde (Reaction 5; $\Delta_RG = -346$ kJ mol^{-1}) (33). Following hydrogen cleavage at the

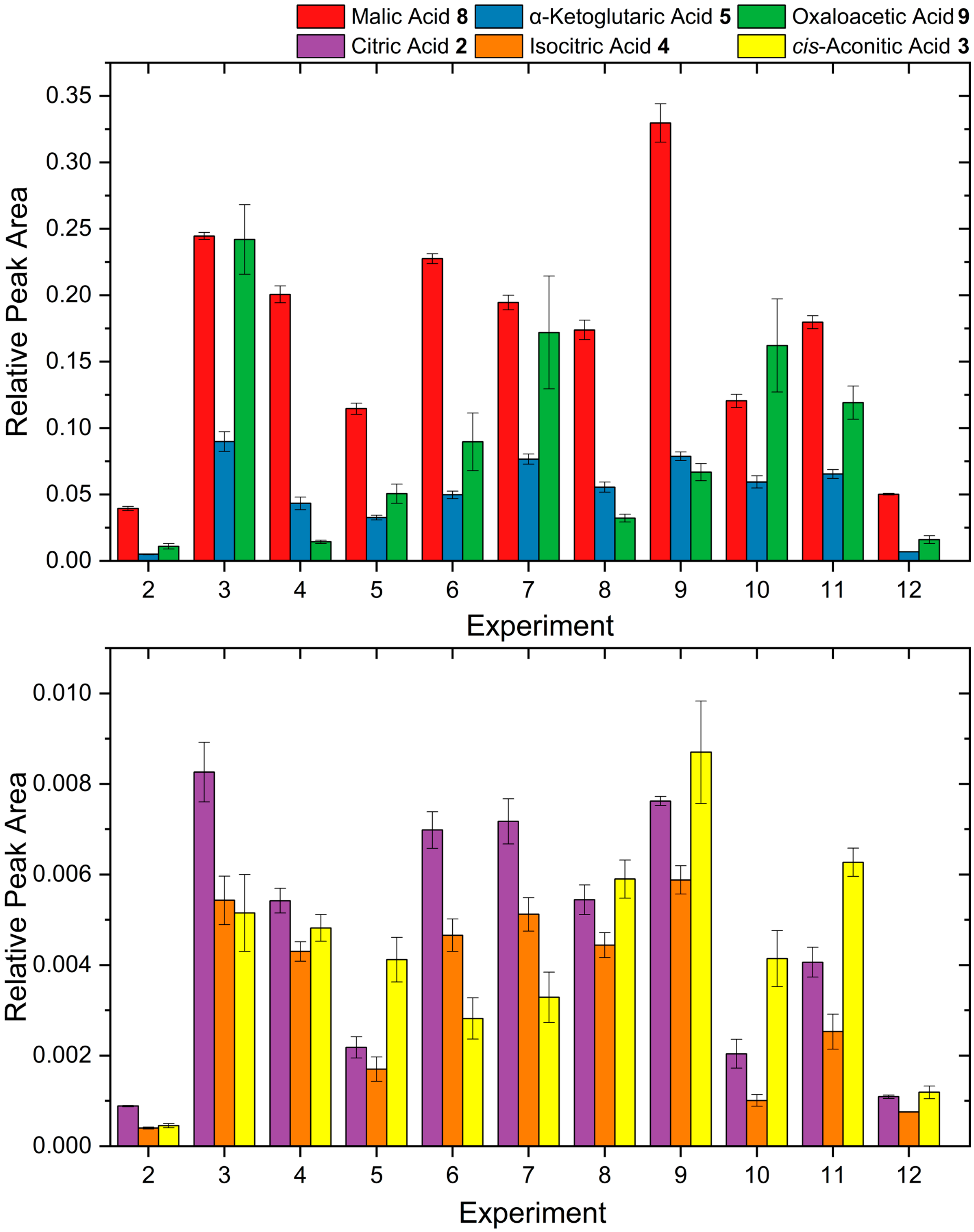

Fig. 4. Quantitative comparison of malic **8**, α-ketoglutaric **5**, oxaloacetic **9**, *cis*-aconitic **3**, citric **2**, and isocitric **4** acids detected in the residues of the exposed interstellar ices. Blank-corrected characteristic peak area relative to the internal standard for each interstellar analog ice experiment; the experiments are defined in *SI Appendix*, Table S1.

aldehyde group (Reaction 6; $\Delta_R G = +367\ \mathrm{kJ\ mol^{-1}}$) (33), this newly generated acetyl radical can undergo barrierless recombination with the hydroxycarbonyl radical to form pyruvic acid **1** (Reaction 7; $\Delta_R G = -336\ \mathrm{kJ\ mol^{-1}}$) (33).

$$\mathrm{CH_4 \rightarrow CH_3 + H} \qquad [1]$$

$$\mathrm{CO_2 \rightarrow CO + O\left(^3P\right)} \qquad [2]$$

$$\mathrm{CO_2 + H \rightarrow HOCO} \qquad [3]$$

$$\mathrm{CO + H \rightarrow HCO} \qquad [4]$$

$$\mathrm{CH_3 + HCO \rightarrow CH_3CHO} \qquad [5]$$

$$\mathrm{CH_3CHO \rightarrow CH_3CO + H} \qquad [6]$$

Table 1. Amounts of malic 8, *cis*-aconitic 3, and citric 2 acids in the interstellar analog ices

		Concentration (ppm)		
Experiment	Ice composition	Malic acid **8**	*cis*-Aconitic acid **3**	Citric acid **2**
1	$^{13}CH_4/^{13}CO_2/^{13}CO/H_2O$ (Blank)	0	0	0
2	$^{13}CH_4/^{13}CO_2$ (2,000 nA, 1 h)	3.7	0.05	0.1
3	$^{13}CH_4/^{13}CO_2$ (5,000 nA, 5 h)	22.6	0.6	1.3
4	$^{13}CH_4/^{13}CO_2/^{13}CO$	18.6	0.5	0.8
5	$^{13}CH_4/^{13}CO_2/^{13}CH_3OH$	10.6	0.5	0.3
6	$^{13}CH_4/^{13}CO_2/H_2O$	21.1	0.3	1.0
7	$^{13}CH_3{}^{13}CH_2OH/^{13}CO_2$	18.0	0.4	1.0
8	$^{13}CH_3{}^{13}CH_2OH/^{13}CO_2/^{13}CH_4$	16.1	0.7	0.8
9	$^{13}CH_3{}^{13}CH_2OH/^{13}CO_2/^{13}CH_4$	30.5	1.0	1.1
10	$^{13}C_2H_6/^{13}CO_2$	11.1	0.5	0.3
11	$^{13}C_2H_6/^{13}CO_2/^{13}CO$	16.6	0.7	0.6
12	$^{13}CO_2/^{13}CH_3{}^{13}CHO$	4.7	0.1	0.2

$$CH_3CO + HOCO \rightarrow CH_3C(O)COOH \qquad \textbf{[7]}$$

To generate more complex acids such as α-ketoglutaric **5** and oxaloacetic acid **9**, pyruvic acid **1** can be used as a starting point since the molecular structure closely resembles the connectivity found within these compounds. By utilizing radicals already present in the ice network such as methyl (CH_3) and hydroxycarbonyl (HOCO), acetic acid (CH_3COOH) can be generated (Reaction 8; $\Delta_R G = -387$ kJ mol^{-1}) (33). Acetic acid, after losing a hydrogen atom in an endoergic reaction, results in the carboxymethyl radical (CH_2COOH; Reaction 9; $\Delta_R G = +408$ kJ mol^{-1}) (33). Similarly, when pyruvic acid **1** loses a hydrogen atom, it forms the carboxy-2-oxoethyl radical ($CH_2C(O)COOH$; Reaction 10). Subsequently, these two radicals—carboxymethyl and carboxy-2-oxoethyl—can recombine to form oxaloacetic acid (**9**, Reaction 11).

$$CH_3 + HOCO \rightarrow CH_3COOH \qquad \textbf{[8]}$$

$$CH_3COOH \rightarrow CH_2COOH + H \qquad \textbf{[9]}$$

$$CH_3C(O)COOH \rightarrow CH_2C(O)COOH + H \qquad \textbf{[10]}$$

$$\begin{gathered} CH_2C(O)COOH + CH_2COOH \rightarrow \\ HOC(O)C(O)CH_2COOH \end{gathered} \qquad \textbf{[11]}$$

To produce α-ketoglutaric acid **5**, a parallel reaction sequence can be proposed by replacing the methyl radical (Reaction 8) with the ethyl radical to produce propanoic acid (CH_3CH_2COOH; Reaction 12; $\Delta_R G = -386$ kJ mol^{-1}) (33). The endoergic cleavage of the carbon-hydrogen bond on propanoic acid leads to the carboxyethyl (CH_2CH_2COOH) radical (Reaction 13), which can undergo a radical–radical recombination with the carboxy-2-oxoethyl radical (Reaction 10) to form α-ketoglutaric acid **5** (Reaction 14).

$$C_2H_2 + HOCO \rightarrow CH_3CH_2COOH \qquad \textbf{[12]}$$

$$CH_3CH_2COOH \rightarrow CH_2CH_2COOH + H \qquad \textbf{[13]}$$

$$\begin{gathered} CH_2CH_2COOH + CH_2C(O)COOH \rightarrow \\ HOC(O)C(O)CH_2CH_2COOH \end{gathered} \qquad \textbf{[14]}$$

Although the FTIR data provide valuable insight into the formation mechanisms of complex acids through the identification of functional groups, several alternative pathways utilizing the same starting material could produce these compounds. Detailed retrosynthetic routes are outlined in Supporting Information deciphering alternative mechanisms to **1**, **5**, and **9** in low-temperature ices (*SI Appendix*, Figs. S16–S52 and Table S37). The process of retrosynthesis illustrates typical formation pathways in interstellar ices which was repeated for all molecules **1** to **9** detected here. These ice experiments represent complex condensed-phase chemistry involving tertiary reactions necessary to produce organic acids. These experiments underscore the ubiquity of forming the carboxylic acid moieties attached to hydrocarbon backbones in interstellar analog ices, utilizing a wide array of reagents. At the core, the carbon-, oxygen-, and hydrogen-rich ices facilitate the production of mono-, di-, and tricarboyxlic acids. Previous work has detailed that these processes can also occur in cases without carbon dioxide, such as in methanol ice matrices (34, 35), but were unable to identify the full suite of acids belonging to the Krebs cycle. This suggests that if these compounds form on interstellar grain surfaces, the abundance of carbon dioxide and the formation of the hydroxycarbonyl radicals are key to producing these acids.

Overall, our study provides compelling evidence for the facile synthesis of the complete suite of carboxylic acids involved in the Krebs cycle: pyruvic acid **1**, citric acid **2**, *cis*-aconitic acid **3**, isocitric acid **4**, *α*-ketoglutaric acid **5**, succinic acid **6**, fumaric acid **7**, malic acid **8**, and oxaloacetic acid **9** (Fig. 1). These acids form in carbon dioxide-containing interstellar analog ices when exposed to proxies of GCRs. The identification of these compounds provides key evidence that these acids, as detected in extraterrestrial sources like Murchison and samples returned from the carbonaceous asteroid Ryugu, represent a potential source of bioavailable material necessary for early metabolic evolution. This model replicates concentrations within these astrophysical objects and supplies an efficacious formation scenario to produce biorelevant carboxylic acids detected therein. Once synthesized abiotically within icy mantles of interstellar dust grains present in dense molecular clouds, they can be incorporated into asteroids, comets, planets, and planetesimals providing the seeds of life to worlds much like our own. These results mark a deeper understanding of interstellar prebiotic evolution; once these acids are delivered to Earth, they could facilitate (geo)chemical processes not unlike the contemporary Krebs cycle through the use of abiotic, nonenzymatic catalysts

(3–8). These results illustrate the interconnected nature of astrophysics, chemistry, and biology in the advent of evolution on early Earth and defines the connection between astrobiology and evolutionary biology. Sugars and amino acids have already been cataloged to form in laboratory interstellar ices and these results expand these biomolecules to include bioenergetic material in the Krebs cycle, further supporting the possibility of life-bearing material produced in interstellar environments. The complex chemistry of these environments sheds light not only on our own evolution but opens the possibility for evolution on other worlds.

Materials and Methods

Surface Scattering Machine. Experiments were performed in a stainless steel ultrahigh-vacuum chamber evacuated to 8×10^{-11} Torr by a magnetically levitated turbomolecular pump (Osaka, TG420MCAC) backed by an oil-free dry scroll pump (Edwards, GVSP30) (23, 36). A cold finger cooled to 10.0 ± 0.3 K by a closed-cycle helium refrigerator (Helix, 9600 Compressor) holds a mirror-polished silver substrate. Twelve sets of experiments were conducted utilizing various gas mixtures of carbon-13 labeled gases: carbon dioxide-^{13}C ($^{13}CO_2$, Sigma Aldrich, 99 atom % ^{13}C), carbon monoxide-^{13}C (^{13}CO, Sigma Aldrich, ≥99 atom % ^{13}C), methane-^{13}C ($^{13}CH_4$, AirGas, >99.9%), methanol-^{13}C ($^{13}CH_3OH$, Sigma Aldrich, >99.9 atom % ^{13}C), ethane-$^{13}C_2$ ($^{13}C_2H_6$, Sigma Aldrich, 99 atom % ^{13}C), ethanol-$^{13}C_2$ ($^{13}CH_3{}^{13}CH_2OH$, Sigma Aldrich, 99 atom % ^{13}C), acetaldehyde-$^{13}C_2$ ($^{13}CH_3{}^{13}CHO$, Sigma Aldrich, 99 atom % ^{13}C), and water (H_2O, HPLC, Fisher Scientific) (see *SI Appendix*, Table S1 for more detail). Two glass capillary arrays were used to introduce gas mixtures into the ultrahigh vacuum chamber to facilitate deposition onto the polished substrate. This process was monitored utilizing interferometry by a HeNe laser (Melles Griot, 25-LHP-230, 632.8 nm) at an angle of incidence of 3° (37). The thickness was calculated based on a weighted average refractive index (*n*) of each ice component (*SI Appendix*, Tables S1 and S2). The relative fractions of reactants were determined using a Fourier Transform infrared (FTIR) spectrometer (Thermo, Nicolet 6700) covering the 6,000 to 500 cm^{-1} range at a spectral resolution of 4 cm^{-1} with a liquid nitrogen cooled HgCdTe (Thermo, MCT-B) detector and each molecules corresponding vibrational band strengths (*SI Appendix*, Table S2).

After the deposition, each sample was isothermally irradiated at 10 K with 5 keV electrons generated by an electron gun (Specs EQ 22-35) at beam currents of 2,000 nA for 1 h for experiment **2** and 5,000 nA for 5 h for experiments **3** to **12** at an angle of 15°. These electrons simulate secondary electrons produced by GCRs. Galactic cosmic ray particles with energies exceeding MeV penetrate through interstellar grains and deposit their energy through inelastic nuclear collisions and electron stopping resulting in displacement of material, ionization, and excitation (38). Ionizations result in a cascade of electrons born of a few keV which initiate nonequilibrium chemical reactions in the icy mantle (39). The maximum depth according to Monte Carlo simulations (CASINO 2.42) (40) is 650 ± 70 nm, which is less than the thickness of the ices (*SI Appendix*, Table S1).

After irradiation, the ices were warmed using a TPD from 10 K to 320 K at a rate of 1 K min^{-1} by a programmable temperature controller (Lakeshore 336). FTIR spectra were collected and averaged in 2-min intervals to monitor thermal and chemical changes.

Two-Dimensional Gas Chromatography Time-of-Flight Mass Spectrometry. The solid residue remaining after the warm-up to room temperature was extracted with 10-times 50 μL of MilliQ® water (Direct 8, 18.2 MΩ cm at 25 °C, <2 ppb total organic carbon, Merck), dried under a gentle stream of nitrogen and converted into *tert*-butyldimethylsilyl (*t*BDMS) derivatives for subsequent two-dimensional gas chromatography time-of-flight mass spectrometry (GC×GC-TOF-MS) analysis. The derivatization step consisted of adding 10 μL of *N,O*-bis(trimethylsilyl) trifluoroacetamide with 1% trimethylsilyl chloride in 25 μL of pyridine to the dried residue, heating at 80 °C for 2 h, followed by cooling to room temperature for 10 min and drying under a gentle stream of nitrogen until approximately 1 to 2 μL of solvent remained, and then 30 μL methyl laurate (internal standard, 10^{-6} M) in hexane was added. The GC×GC column set consisted of a DB-5ms Ultra Inert primary column (29.66 m × 0.25 mm, 0.25 μm, Agilent, CA) coupled by a Press-Tight connector (Restek, Bellefonte, PA) to a DB Wax (polyethylene glycol, 1.2 m × 0.1 mm, 0.1 μm, Agilent, CA) secondary column. Modulation was achieved through a dual-stage thermal jet modulator using liquid nitrogen. Hydrogen was used as carrier gas at a flow rate of 1.5 mL/min. The inlet was held at 245 °C, and the transfer line and the ion source at 250 °C and 240 °C, respectively. The temperature of the primary oven was held at 40 °C for 1 min, followed by an increase of 5 °C/min to 235 °C, where it was held for 15 min. Secondary oven operated with a constant 5 °C offset with respect to the primary oven, modulator offset was 5 °C with respect to the secondary oven, and the modulation period was 5 s. The TOF-MS operated at 150 Hz storage rate with a 50 to 650 amu mass range and a 15-min solvent delay. The microchannel plate detector voltage was kept at 2,036 V. Aliquots of 1 μL of the derivatized mixtures were injected three times in splitless mode. For the identification of compounds in the interstellar ice analog residue, individual reference standards of pyruvic, succinic, fumaric, L-malic, α-ketoglutaric, oxaloacetic, *cis*-aconitic, and citric acids (Sigma Aldrich, highest available purity, 5×10^{-9} M; 5×10^{-8} M; 5×10^{-7} M; 5×10^{-6} M; and 5×10^{-5} M) were prepared and analyzed analogously.

Data, Materials, and Software Availability. All study data are included in the article and/or *SI Appendix*.

ACKNOWLEDGMENTS. The work at the University of Hawaii was funded by the US NSF Division of Astronomical Sciences, under grant AST-2403867. C.M. acknowledges funding from the Simone and Cino Del Duca Foundation–Institut de France as well as the European Research Council under the European Union's Horizon 2020 research and innovation program (grant agreement 804144). We would like to thank Yvonne Chan and Ethan Hill for advocacy and mentoring. We would also like to thank Kaelyn Pacpaco for her involvement in this work.

1. H. A. Krebs, W. A. Johnson, The role of citric acid in intermediate metabolism in animal tissues. *FEBS Lett.* **117**, K1–K10 (1980).
2. E. Meléndez-Hevia, T. G. Waddell, M. Cascante, The puzzle of the Krebs citric acid cycle: Assembling the pieces of chemically feasible reactions, and opportunism in the design of metabolic pathways during evolution. *J. Mol. Evol.* **43**, 293–303 (1996).
3. M. A. Keller, D. Kampjut, S. A. Harrison, M. Ralser, Sulfate radicals enable a non-enzymatic Krebs cycle precursor. *Nat. Ecol. Evol.* **1**, 0083 (2017).
4. G. Springsteen, J. R. Yerabolu, J. Nelson, C. J. Rhea, R. Krishnamurthy, Linked cycles of oxidative decarboxylation of glyoxylate as protometabolic analogs of the citric acid cycle. *Nat. Commun.* **9**, 91 (2018).
5. M. Yadav, S. Pulletikurti, J. R. Yerabolu, R. Krishnamurthy, Cyanide as a primordial reductant enables a protometabolic reductive glyoxylate pathway. *Nat. Chem.* **14**, 170–178 (2022).
6. R. T. Stubbs, M. Yadav, R. Krishnamurthy, G. Springsteen, A plausible metal-free ancestral analogue of the Krebs cycle composed entirely of α-ketoacids. *Nat. Chem.* **12**, 1016–1022 (2020).
7. K. B. Muchowska *et al.*, Metals promote sequences of the reverse Krebs cycle. *Nat. Ecol. Evol.* **1**, 1716–1721 (2017).
8. K. B. Muchowska, S. J. Varma, J. Moran, Synthesis and breakdown of universal metabolic precursors promoted by iron. *Nature* **569**, 104–107 (2019).
9. G. Cooper, C. Reed, D. Nguyen, M. Carter, Y. Wang, Detection and formation scenario of citric acid, pyruvic acid, and other possible metabolism precursors in carbonaceous meteorites. *Proc. Natl. Acad. Sci. U.S.A.* **108**, 14015–14020 (2011).
10. Y. Takano *et al.*, Primordial aqueous alteration recorded in water-soluble organic molecules from the carbonaceous asteroid (162173) Ryugu. *Nat. Commun.* **15**, 5708 (2024).
11. J. R. Cronin, S. Chang, "Organic matter in meteorites: Molecular and isotopic analyses of the Murchison meteorite" in *The Chemistry of Life's Origins*, J. M. Greenberg, C. X. Mendoza-Gómez, V. Pirronello, Eds. (Springer Netherlands, 1993), vol. 209, pp. 209–258.
12. N. F. W. Ligterink *et al.*, The rapid formation of macromolecules in irradiated ice of protoplanetary disk dust traps. *Nat. Astron.* **8**, 1257–1263 (2024).
13. T. Hama, N. Watanabe, Surface processes on interstellar amorphous solid water: Adsorption, diffusion, tunneling reactions, and nuclear-spin conversion. *Chem. Rev.* **113**, 8783–8839 (2013).
14. M. J. Abplanalp *et al.*, A study of interstellar aldehydes and enols as tracers of a cosmic ray-driven nonequilibrium synthesis of complex organic molecules. *Proc. Natl. Acad. Sci. U.S.A.* **113**, 7727–7732 (2016).
15. C. Meinert *et al.*, Ribose and related sugars from ultraviolet irradiation of interstellar ice analogs. *Science* **352**, 208–212 (2016).
16. P. D. Holtom, C. J. Bennett, Y. Osamura, N. J. Mason, R. I. Kaiser, A combined experimental and theoretical study on the formation of the amino acid glycine (NH_2CH_2COOH) and its isomer ($CH_3NHCOOH$) in extraterrestrial ices. *Astrophys. J.* **626**, 940 (2005).
17. G. M. Muñoz Caro *et al.*, Amino acids from ultraviolet irradiation of interstellar ice analogues. *Nature* **416**, 403–406 (2002).
18. N. F. Kleimeier, A. K. Eckhardt, P. R. Schreiner, R. I. Kaiser, Interstellar formation of biorelevant pyruvic acid ($CH_3COCOOH$). *Chem* **6**, 3385–3395 (2020).
19. M. K. McClure *et al.*, An Ice Age JWST inventory of dense molecular cloud ices. *Nat. Astron.* (2023).

20. M. Agúndez, V. Wakelam, Chemistry of dark clouds: Databases, networks, and models. *Chem. Rev.* **113**, 8710–8737 (2013).
21. M. S. El-Nawawy, D. A. Howe, T. J. Millar, Chemical evolution in collapsing cores. *Mon. Not. R. Astron. Soc.* **292**, 481–489 (1997).
22. A. Bergantini, S. Góbi, M. J. Abplanalp, R. I. Kaiser, A mechanistical study on the formation of dimethyl ether (CH_3OCH_3) and ethanol (CH_3CH_2OH) in methanol-containing ices and implications for the chemistry of star-forming regions. *Astrophys. J.* **852**, 70 (2018).
23. C. J. Bennett, C. S. Jamieson, Y. Osamura, R. I. Kaiser, Laboratory studies on the irradiation of methane in interstellar, cometary, and solar system ices. *Astrophys. J.* **653**, 792 (2006).
24. C. J. Bennett, Y. Osamura, M. D. Lebar, R. I. Kaiser, Laboratory studies on the formation of three C2H4O isomers—Acetaldehyde (CH_3CHO), ethylene oxide (c-C_2H_4O), and vinyl alcohol (CH_2CHOH)—in interstellar and cometary ices. *Astrophys. J.* **634**, 698 (2005).
25. P. A. Gerakines, W. A. Schutte, J. M. Greenberg, E. F. van Dishoeck, The infrared band strengths of H_2O, CO and CO_2 in laboratory simulations of astrophysical ice mixtures. *Astron. Astrophys.* **296**, 810 (1995).
26. G. Socrates, *Infrared and Raman Characteristic Group Frequencies: Tables and Charts* (John Wiley & Sons, 2004).
27. W. Hagen, A. Tielens, J. Greenberg, The infrared spectra of amorphous solid water and ice I_c between 10 and 140 K. *J. Chem. Phys.* **56**, 367–379 (1981).
28. M. Bajo-Fernández *et al.*, Structural elucidation of derivatives of polyfunctional metabolites after methyl chloroformate derivatization by high-resolution mass spectrometry gas chromatography. Application to microbiota metabolites. *J. Chromatogr. A* **1717**, 464656 (2024).
29. P. Hušek *et al.*, Profiling of urinary amino-carboxylic metabolites by in-situ heptafluorobutyl chloroformate mediated sample preparation and gas chromatography-mass spectrometry. *J. Chromatogr. A* **1443**, 211–232 (2016).
30. O. Mamer *et al.*, The complete targeted profile of the organic acid intermediates of the citric acid cycle using a single stable isotope dilution analysis, sodium borodeuteride reduction and selected ion monitoring GC/MS. *Metabolomics* **9**, 1019–1030 (2013).
31. M. K. McClure *et al.*, An Ice Age JWST inventory of dense molecular cloud ices. *Nat. Astron.* **7**, 431–443 (2023).
32. C. J. Bennett, C. S. Jamieson, R. I. Kaiser, Mechanistical studies on the formation and destruction of carbon monoxide (CO), carbon dioxide (CO_2), and carbon trioxide (CO_3) in interstellar ice analog samples. *Phys. Chem. Chem. Phys.* **12**, 4032–4050 (2010).
33. B. Ruscic, D. Bross, *Active Thermochemical Tables (ATcT) values based on ver. 1.122 of the Thermochemical Network* (Argonne National Laboratory, 2019).
34. C. Zhu, A. M. Turner, C. Meinert, R. I. Kaiser, On the production of polyols and hydroxycarboxylic acids in interstellar analogous ices of methanol. *Astrophys. J.* **889**, 134 (2020).
35. S. Maity, R. I. Kaiser, B. M. Jones, Formation of complex organic molecules in methanol and methanol–carbon monoxide ices exposed to ionizing radiation—A combined FTIR and reflectron time-of-flight mass spectrometry study. *Phys. Chem. Chem. Phys.* **17**, 3081–3114 (2015).
36. C. J. Bennett, C. Jamieson, A. M. Mebel, R. I. Kaiser, Untangling the formation of the cyclic carbon trioxide isomer in low temperature carbon dioxide ices. *Phys. Chem. Chem. Phys.* **6**, 735–746 (2004).
37. A. M. Turner *et al.*, A photoionization mass spectroscopic study on the formation of phosphanes in low temperature phosphine ices. *Phys. Chem. Chem. Phys.* **17**, 27281–27291 (2015).
38. J. F. Ziegler, J. M. Manoyan, The stopping of ions in compounds. *Nucl. Instrum. Methods Phys. Res. B* **35**, 215–228 (1988).
39. R. I. Kaiser, K. Roessler, Theoretical and laboratory studies on the interaction of cosmic-ray particles with interstellar ices. III. Suprathermal chemistry-induced formation of hydrocarbon molecules in solid methane (CH_4), ethylene (C_2H_4), and acetylene (C_2H_2). *Astrophys. J.* **503**, 959–975 (1998).
40. D. Drouin *et al.*, CASINO V2.42—A fast and easy-to-use modeling tool for scanning electron microscopy and microanalysis users. *Scanning* **29**, 92–101 (2007).